

AD-A040 777

AIR FORCE GEOPHYSICS LAB HANSCOM AFB MASS  
ROCKET MEASUREMENT OF THE ENERGY DISTRIBUTION AND FLUX OF THERM--ETC(U)  
JAN 77 W J MCMAHON, L HEROUX  
AFGL-TR-77-0013

F/G 4/1

UNCLASSIFIED

NL

1 OF 1

AD  
A040777



END

DATE  
FILMED  
7-77

AD A 040777

AFGL-TR-77-0013  
ENVIRONMENTAL RESEARCH PAPERS, NO. 589

12  
B.S.



## Rocket Measurement of the Energy Distribution and Flux of Thermospheric Photoelectrons

W.J. McMAHON  
L. HEROUX

13 January 1977

Approved for public release; distribution unlimited.

JUN 21 1977  
B

AERONOMY DIVISION PROJECT 6688  
AIR FORCE GEOPHYSICS LABORATORY  
HANSCOM AFB, MASSACHUSETTS 01731

AIR FORCE SYSTEMS COMMAND, USAF

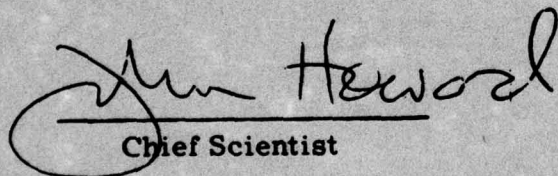


AD No. \_\_\_\_\_  
DDC FILE COPY

This report has been reviewed by the ESD Information Office (OI) and is releasable to the National Technical Information Service (NTIS).

This technical report has been reviewed and is approved for publication.

FOR THE COMMANDER

  
Chief Scientist

Qualified requestors may obtain additional copies from the Defense Documentation Center. All others should apply to the National Technical Information Service.



Unclassified

SECURITY CLASSIFICATION OF THIS PAGE (When Data Entered)

REPORT DOCUMENTATION PAGE		READ INSTRUCTIONS BEFORE COMPLETING FORM
1. REPORT NUMBER	2. GOVT ACCESSION NO.	3. RECIPIENT'S CATALOG NUMBER
AFGL-TR-77-0013, AFGL-ERP-589		
4. TITLE (and Subtitle)	5. TYPE OF REPORT & PERIOD COVERED	
ROCKET MEASUREMENT OF THE ENERGY DISTRIBUTION AND FLUX OF THERMOSPHERIC PHOTOELECTRONS.	Scientific. Interim.	
7. AUTHOR(s)	6. PERFORMING ORG. REPORT NUMBER	
W. J. /McMahon L. /Heroux	ERP No. 589 ✓	
9. PERFORMING ORGANIZATION NAME AND ADDRESS	8. CONTRACT OR GRANT NUMBER(s)	
Air Force Geophysics Laboratory (LK) Hanscom AFB, Massachusetts 01731		
11. CONTROLLING OFFICE NAME AND ADDRESS	10. PROGRAM ELEMENT, PROJECT, TASK AREA & WORK UNIT NUMBERS	
Air Force Geophysics Laboratory (LK) Hanscom AFB, Massachusetts 01731	16 62101F 12 06 66880601	
14. MONITORING AGENCY NAME & ADDRESS (if different from Controlling Office)	12. REPORT DATE	
Environmental research papers	13 January 1977	
	13. NUMBER OF PAGES	
	28	
	15. SECURITY CLASS. (of this report)	
	Unclassified	
	15a. DECLASSIFICATION/DOWNGRADING SCHEDULE	
16. DISTRIBUTION STATEMENT (of this Report)		
Approved for public release; distribution unlimited.		
17. DISTRIBUTION STATEMENT (of the abstract entered in Block 20, if different from Report)		
18. SUPPLEMENTARY NOTES		
19. KEY WORDS (Continue on reverse side if necessary and identify by block number)		
Thermospheric photoelectrons Low energy electron spectra Aeronomy Atmosphere		
20. ABSTRACT (Continue on reverse side if necessary and identify by block number)		
An electron analyzer of the 127° cylindrical electrostatic deflection type, designed to measure the energy distribution and flux of thermospheric photoelectrons in the energy range from near zero to 100 eV, has been successfully flown on a rocket probe. The design and operational characteristics of the instrument are briefly described and the importance of full calibration procedures discussed. Methods for correcting or minimizing the effects of vehicle-induced disturbance of the environment being measured were incorporated into the experiment. These included correction for the energy → next page		

DD FORM 1 JAN 73 1473 EDITION OF 1 NOV 65 IS OBSOLETE

Unclassified

SECURITY CLASSIFICATION OF THIS PAGE (When Data Entered)

409 578

LB



Unclassified

SECURITY CLASSIFICATION OF THIS PAGE(When Data Entered)

20. (Cont)

attenuation and refractive signal losses which are the dual effects of vehicle skin charge. Photoelectron spectra in the energy range 2 to 100 eV were measured over an altitude range of 100 to 220 km during the first flight of the instrument. These spectra display distinct features that are consistent with the most recently developed theory,\* and similar to those obtained in the latest observations published.† The valley-like structure in the energy range 2 to 5 eV, attributed to the resonant vibrational excitation of  $N_2^+$ , was observed in somewhat more detail and over a greater altitude range than previously seen. Improved in situ observation of this feature appears to have the potential of providing useful information relating to important thermospheric parameters such as the vibrational temperature and neutral density of  $N_2$ .

\*Victor, G. A., Kirby-Docken, K., and Dalgarno, A. (1976) Planet. Space Sci. 24:679; Jasperse, J. R., Planet. Space Sci. (to be published).

†Doering, J. P., Peterson, W. K., Bostrom, C. O., and Potemra, R. A. (1976) Geophys. Res. Lett. 3:129.

Unclassified

SECURITY CLASSIFICATION OF THIS PAGE(When Data Entered)

## Contents

1. INTRODUCTION	5
2. THE FLIGHT ANALYZER	6
3. THE ROCKET PAYLOAD	10
4. CALIBRATION OF THE ANALYZER	11
5. VEHICLE INDUCED INTERFERENCE	13
6. FLIGHT RESULTS	16
7. DISCUSSION	19
REFERENCES	25
APPENDIX A: Correction for Refractive Signal Losses Due to Vehicle Skin Charge	27

## Illustrations

1. Cross Section through Focusing Plane of the Electron Energy Analyzer	8
2. Photograph of Two Partially Assembled Flight Instruments	9
3. Rocket Payload Configuration Showing the Electron Analyzer Mounted on Rear Section of the EUV Spectrometer	11

## Illustrations

4. Illustration of Signal Loss Caused by the Refraction of Environmental Electrons during Passage through the Space Charge Sheath Surrounding a Planar Aperture	15
5. Photograph of the Payload Mounted in the Nose Section of an Aerobee 170 Prior to Flight	16
6. Example of Raw Data Readout Showing 12 Complete Energy Scans	17
7. Photoelectron Flux as a Function of Electron Energy for Several Altitudes	19
8. Comparison of the Present Results with Those Obtained by Others for the 180 to 200-km Altitude Region	20
9. Energy Spectra between 2 and 5.6 eV as a Function of Altitude	22
10. Ratios of Peak-to-Valley Photoelectron Flux as a Function of Altitude	24

## Tables

1. Comparison of Experimental Details for Six Measurements of Electron Energy Spectra in the ~180 to 200-km Altitude	21
--	----



ACCESSION for	
RTIS	White Section <input checked="" type="checkbox"/>
BDC	Buff Section <input type="checkbox"/>
UNANNOUNCED	<input type="checkbox"/>
JUSTIFICATION	
BY	
DISTRIBUTION/AVAILABILITY CODES	
In . . . and/or SPECIAL	
A	

## Rocket Measurement of the Energy Distribution and Flux of Thermospheric Photoelectrons

### 1. INTRODUCTION

Ionospheric electrons produced by photoionization of atmospheric gases play a major role in several upper atmospheric processes such as the production of air-glow radiation and heating. Knowledge of the energy distribution and density of atmospheric photoelectrons is necessary to an understanding of these processes. Several theoretical studies of thermospheric photoelectrons conducted in recent years are compared by Cicerone et al.<sup>1</sup> A theoretical study by Ashihara and Takayanagi<sup>2</sup> concentrated on the energy region below 8.7 eV while Victor et al.<sup>3</sup> and Jasperse<sup>4</sup> have carried out the most recent calculations of the photoelectron flux in the energy range to 70 and 210 eV, respectively. Reliable experimental data are sparse, however, because of the difficulty inherent in the in situ detection and measurement of these low energy electrons.

Recently, some significant structural details have begun to emerge. Mukai and Hirao,<sup>5</sup> who used an electron analyzer in a rocket probe, and Doering et al.,<sup>6</sup> who used an analyzer on the AE-C satellite, have to varying degrees observed structure in the energy spectra in the range 20 to 30 eV. This structure in the energy distribution is attributed to the ionization of atomic oxygen and molecular nitrogen by the HeII solar emission line at 304 Å. A later experiment by Doering et al.<sup>7</sup> aboard the AE-E satellite showed this structure with improved energy resolution, as well as

(Received for publication 11 January 1977)

(Because of the large number of references cited above, they will not be listed here. See References, Page 25, for References 1 through 7.)

additional structure in the form of a trough, or valley, in the energy region 2 to 4 eV. The latter feature is attributed to electron energy loss due to vibrational excitation of  $N_2$ . Hays and Sharp<sup>8</sup> had earlier observed a similar valley in segments of electron spectra obtained in a rocket flight. Although the recent data indicate a trend toward increasing agreement between theoretical calculations and between experiment and theory, discrepancies still remain. Important gaps in the present knowledge of ionospheric photoelectron fluxes must be filled chiefly by more accurate in situ measurements.

This report describes an electron energy analyzer designed for rocket measurements of thermospheric electrons in the energy range from near zero to 100 eV. The problems of environmental disturbances induced by the rocket probe, common to any such measurements, are discussed. The results from the first flight of this instrument are shown to be similar to the latest experimental results of Doering et al<sup>7</sup> and to be consistent with the most recently developed theory. These data also show low energy structural detail in the range 2 to 4 eV that is somewhat more pronounced, and which persists to altitudes lower than observed by others.

The electron analyzer was flown in a rocket payload that also included a solar pointed extreme ultraviolet (EUV) spectrometer for measurement of solar fluxes and a photometer for measurement of airglow radiation in the second-positive band of  $N_2$  at 3371 Å. The mounting of the analyzer on the spectrometer was important to its in-flight orientation with respect to the geomagnetic field, and the payload package is described only in reference to this orientation. Otherwise this report is restricted to a discussion of the electron energy analyzer and the data obtained by it.

## 2. THE FLIGHT ANALYZER

There are a variety of methods by which electron energy distributions may be measured, although not all are appropriate for low energy measurements, or for space flight application. The two experimental groups<sup>5,6</sup> which have observed significant structural detail in their spectra employed 180° spherical electrostatic deflection instruments, the application of a method introduced by Purcell<sup>9</sup> and developed by Simpson<sup>10</sup> and others<sup>11</sup> for various laboratory studies. We have used

8. Hays, P. B., and Sharp, W. E. (1973) Twilight airglow photoelectrons and [OI] 5577-angstrom radiation, *J. Geophys. Res.* 78:1153.
9. Purcell, E. M. (1938) The focusing of charged particles by a spherical condenser, *Phys. Res.* 54:818.
10. Simpson, J. A. (1964) High resolution, low energy electron spectrometer, *Rev. Sci. Instrum.* 35:1698.
11. Kuyatt, C. E., and Simpson, J. A. (1967) Electron monochromator design, *Rev. Sci. Instrum.* 38:103.

the 127° cylindrical electrostatic deflection technique first developed by Hughes and Rojansky.<sup>12</sup> A detailed evaluation of these two methods, as well as a comparison of them with other techniques of electron spectrometry, is given by Roy and Carette.<sup>13</sup> Although the transmission efficiencies of the 180° analyzers are superior to those of the 127° instrument, their characteristics are otherwise comparable for space probe applications. Our choice of the 127° analyzer was based on: (1) an instrument configuration more readily adaptable to presentation of the entrance aperture as part of a relatively large planar surface (significance to be discussed later); (2) ease of fabrication and assembly of the flight instrument; and (3) space limitations imposed by the rocket payload. The design of this instrument was influenced by previous work with 127° analyzers carried out in this laboratory.<sup>14</sup>

A cross section drawing of the flight instrument through its focusing plane is shown in Figure 1. It consists basically of a collimating aperture and slit assembly a, the analyzer deflection plate assembly b, a detector c, a magnetic shield enclosure d, and an aperture field plate e. Energy dependent focusing which takes place in the radial electric field of the analyzer between the outer  $p_o$  and inner  $p_i$  deflection plates is a function of the voltage differential applied between them. Theoretically, a line object at the entrance slit  $s_1$  is brought to focus as a line image at the exit slit  $s_2$  after deflection through  $\pi/\sqrt{2}$  radians (127.28°). A sawtooth serration, 0.005 in. deep, is machined into the inner surfaces of both deflection plates to reduce specular reflections. The detector is a modified Galileo Corporation Model 4028 channel electron multiplier (CEM) having a gain of  $10^8$  at 3 kV. The CEM was coupled to a pulse amplifier and operated as an electron counter. The counting system, which exhibited a well-defined plateau, was operated well beyond the onset of the plateau; a dark count rate of less than 0.5 cps was typical. The CEM is potted in RTV-1 compound and enclosed in a Kel-F block assembly. Its mounting at the exit slit is such that the cone axis is offset 20° from the normal to the exit slit plane to ensure that all focused electrons strike the inner surface of the cone. The entire instrument is enclosed by a Co-Netic magnetic shield (d in Figure 1). The energy resolution of the analyzer defined as  $\Delta E/E$ , where  $E$  is the energy of the electrons brought to a focus and  $\Delta E$  the instrumental energy bandwidth, was designed to be 10 percent for the initial flight instrument. This characteristic can be improved by simple design changes in later models. The calculated acceptance angles are  $\pm 5.2^\circ$  with respect to the width of the entrance

12. Hughes, A.L., and Rojansky, V. (1929) On the analysis of electron velocities, by electrostatic means, Phys. Res. 34:284.

13. Roy, D., and Carette, J.D. (1971) Electrostatic spectrometers, Part II, Can. J. Phys. 49:2138.

14. McMahon, W., and Heroux, L. (1974) Measurement of energy and angular distribution and extreme ultraviolet photoelectrons, Appl. Opt. 13:438.



slit (focusing plane) and  $\pm 6.9^\circ$  with respect to its height. The calculated geometric factor, given by the product of the effective area  $A$  and solid angle  $\Omega$  of the entrance aperture, is  $2.86 \times 10^{-3} \text{ cm}^2 \text{ ster}$ . The actual values of this parameter can be determined only by careful laboratory calibration, as will be discussed later.

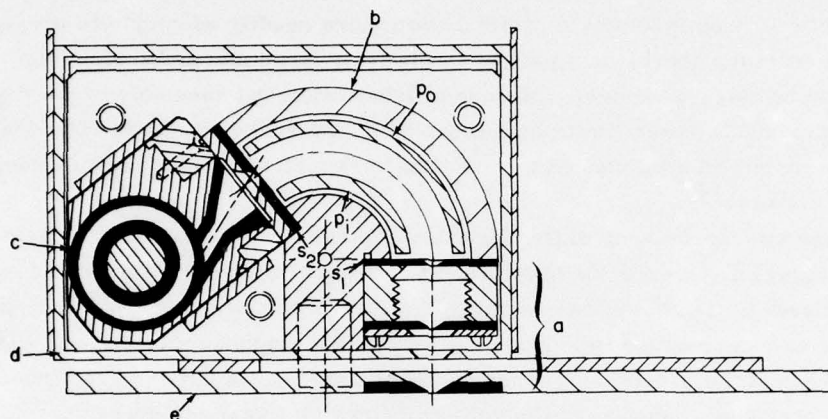


Figure 1. Cross Section through Focusing Plane of the Electron Energy Analyzer: (a) Collimating Aperture Assembly; (b) the  $127^\circ$  Deflection Analyzer Assembly; (c) the Detector Assembly; (d) the Magnetic Shield Enclosure; and (e) the Aperture Field Plate. The analyzer entrance slit which is also the field stop is indicated by  $s_1$  and the exit slit by  $s_2$ . The inner and outer deflection plates are indicated by  $p_1$  and  $p_0$ .

Figure 2 shows two instruments in two different stages of partial assembly. The deflector plates and associated structure are shown at the upper left; the entrance and exit slit assemblies are laid out below the deflector plate; and the CEM is shown enclosed in its mounting assembly and aligned with the exit slit. A more completely assembled analyzer is shown at the right of the figure. This assembly also includes a printed circuit board frame on which the high voltage power supply and preamplifier circuits are later mounted. The instrument wiring and magnetic shield enclosure are not shown in the photograph.

The voltage differential  $V_A$  applied to the deflector plates determines the energy  $E$  of the electrons brought to focus within the bandwidth  $\Delta E$  of the analyzer. This analyzer voltage is applied as plus and minus  $1/2 V_A$  to the inner and outer plates, respectively, ensuring that electrons which follow a central trajectory in the analyzer travel along a nearly zero equipotential path with respect to the instrument slit faces which are at vehicle ground. For the first flight, an energy range from approximately 1 to 100 eV was scanned by varying  $V_A$  in 64 discrete steps every

1.28 seconds. Except for the first 12 steps, the incremental energy increase for each successive step was slightly less than the energy bandwidth of the analyzer. This eliminated gaps in the measured spectra over the energy range 4.6 to 100 eV. For the first 12 steps that sampled the energy range between 1 and 4.6 eV, gaps in the measured spectra were necessary to allow extension of the range to 100 eV in 64 steps. The design of the electronics is sufficiently flexible so that stepped voltage increments and the corresponding energy parameters can be varied for future flights.

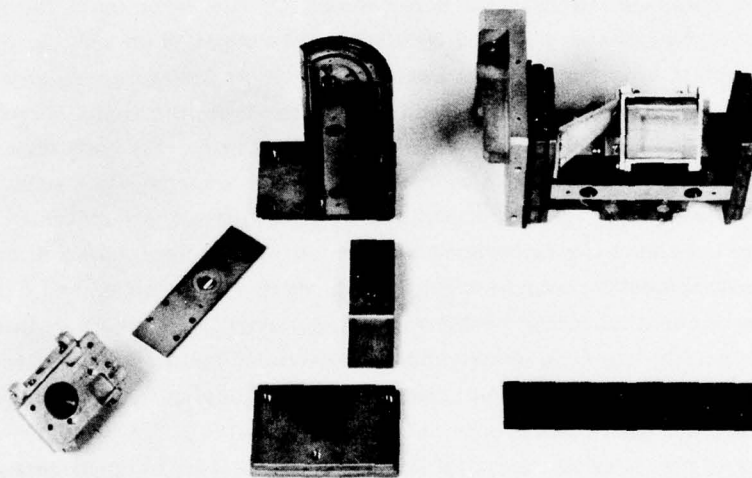


Figure 2. Photograph of Two Partially Assembled Flight Instruments. The deflection plate assembly and associated structure is shown at the upper left. The entrance and exit slit assemblies are laid out below the deflector assembly. The CEM detector, enclosed in its mounting assembly, is positioned in line with the exit slit. Below the entrance slit is one of two end plates over which the magnetic shield is mounted. The analyzer in a more advanced state of assembly is shown, exit face up, at the right. Installed diagonally between the detector assembly and one end plate is a printed circuit board on which the high voltage power supply and preamplifier circuits are later mounted. The magnetic shield enclosure, the aperture field plate, and instrument wiring are not shown

### 3. THE ROCKET PAYLOAD

The electron analyzer was flown in a rocket payload that contained a solar (EUV) spectrometer mounted on a biaxial pointing control that directed the entrance aperture of the spectrometer at the center of the solar disk. The electron analyzer was attached to the rear surface of the EUV spectrometer so that the aperture of the analyzer was aligned in an approximately antisolar direction during the period of data acquisition. The experiment configuration is illustrated in Figure 3, which shows the electron analyzer and spectrometer in the stowed position but with the rocket nose cone raised, and in the deployed position with the spectrometer pointing at the sun. This configuration provides an almost ideal platform for the electron energy analyzer for two reasons: First, since the electron analyzer is oriented in the antisolar direction throughout the data acquisition period, its aperture is shielded from solar radiation. This solar shaded position eliminates the cyclic and substantial data degradation suffered by instruments mounted on spin stabilized space vehicle platforms during those periods when the entrance aperture and nearby components are sunlit. Photoelectrons generated from the sunlit components in the vicinity of the analyzer aperture can saturate or severely contaminate the analyzer signal. Moreover, it is extremely difficult to correct for such contamination, since the energy spectra of photoelectrons emitted from materials commonly used to construct the instrument and vehicle can be deceptively similar to that of the environmental photoelectrons, as shown by Feuerbacher and Fitton.<sup>15</sup> Secondly, the present mounting configuration can virtually eliminate geomagnetic shadowing, since the electron spectrometer essentially maintains a constant orientation with respect to the geomagnetic field lines during flight. Under the right circumstances, the field lines can be held nearly parallel to the entrance-slit normal. For flights near midday, the local hour angle (LHA) approaches zero, and the magnetic declination of the launch site then becomes the significant angular component of the field in the horizontal plane. A LHA aligned with the declination by planned launch timing yields zero angular departure in this plane. Furthermore, for mid-latitude launch sites, the near midday solar zenith angle (SZA) can be nearly equal to the magnetic inclination (dip angle), resulting in minimal angular departure from the field in the vertical plane. In this case, electrons within the solid acceptance angle of the analyzer aperture will have very small pitch angles (angle between magnetic and electron velocity vectors) and experience no geomagnetic shadowing by the payload or vehicle components. For flights planned where the LHA or SZA are substantially nonparallel to the geomagnetic declination or inclination, such as near morning or evening twilights, or at polar or equatorial

15. Feuerbacher, B., and Fitton, B. (1972) Experimental investigation of photoemission from satellite surface materials, J. Appl. Phys. 43:1563.



launch sites, it is possible to reorient the electron analyzer with respect to the solar pointing control deployment axis so as to approach parallel orientation between the analyzer axis and magnetic field while still maintaining the analyzer aperture in a sunshaded position.

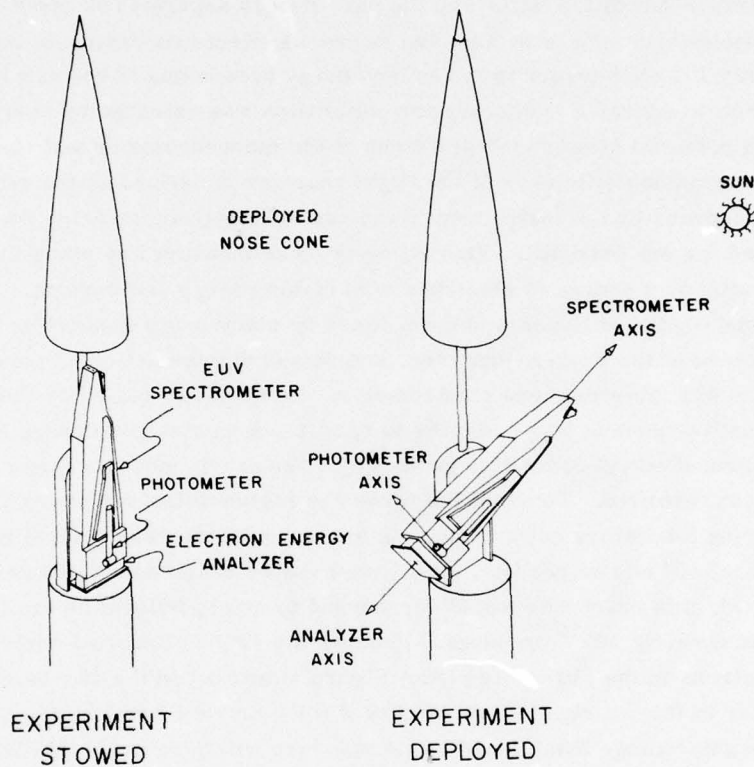


Figure 3. Rocket Payload Configuration Showing the Electron Analyzer Mounted on Rear Section of the EUV Spectrometer. The experimental package is shown in the stowed position but with nose cone raised at the left of figure, and in the deployed position at the right.

#### 4. CALIBRATION OF THE ANALYZER

A determination of the energy scale, energy resolution, transmission efficiency, and geometric factor of the electron analyzer is necessary to convert the raw data obtained in flight to meaningful values of photoelectron flux. With the exception of the geometric factor  $A\Omega$ , these parameters were measured in the laboratory by

using a  $127^\circ$  electron analyzer of a design described by Kerwin et al<sup>16</sup> as an electron monochromator. This monochromator has a filament assembly mounted at its entrance slit in order to provide a thermionic source of electrons; it also has deflection plates constructed of high transparency mesh that are backed by exterior plates biased to +45 V for elimination of space charge effects. The monochromator and flight analyzer were mounted in tandem with the exit slit of the former aligned with the entrance slit of the latter and the pair of slits separated by about 0.25 inch. The monochromator was adjusted to provide electrons having an initial energy of only 1.3 eV in order to minimize energy broadening of the exit beam. The range of electron energies necessary for calibration was extended by applying an accelerating potential between the slit faces of the monochromator and analyzer.

The transmission efficiency of the flight analyzer is defined as the ratio of the count rate recorded by the instrument to the rate of electrons entering its active region behind the entrance slit. This efficiency was measured by using the electron monochromator as a source of electrons of variable energy and current. The electron rate entering the analyzer was determined by electrically connecting both deflection plates of the passive analyzer, and measuring the collected current with a Cary Model 401 vibrating reed electrometer. Immediately following this measurement, the instrument was activated to operate as an electron energy analyzer and the integrated output count rate produced by the nearly monoenergetic input electron beam recorded. To avoid the nonlinear region of the analyzer CEM detector during laboratory calibration, the output count rate was limited to values less than about  $10^5$  counts per sec. If a transmission efficiency of 100 percent were assumed, this count rate would correspond to an upper limit on the input current of approximately  $10^{-14}$  amperes. Because the  $127^\circ$  cylindrical analyzer focuses electrons in the slit-width plane (Figure 1) and not in the slit-height plane perpendicular to this, a significant fraction of the electrons entering the analyzer within the angular range established by its aperture will have paths that fall outside of the exit slit height limits and will not be recorded. This effectively lowers the transmission efficiency of a  $127^\circ$  analyzer and, therefore allows an increase in the upper limit of the current input to values near  $10^{-13}$  amperes. The transmission efficiency of the analyzer was measured by varying the input current for a fixed energy over the range  $10^{-13}$  to  $10^{-15}$  amperes. The efficiency was constant to within 10 percent over this current range, which corresponded to a range of output count rates from about  $10^5$  to  $10^3$  counts per sec. The signal count rate recorded during the flight of the analyzer was in general less than  $5 \times 10^4$  counts per sec, so that a linear relationship between the recorded counting rate and the

16. Kerwin, L., Marmet, P., and Carotte, J.D. (1969) High resolution electron beams and their application, in *Case Studies in Atomic Physics I*, by E.W. McDaniel and M.R.C. McDowell, Ed., North-Holland Publishing Co., Amsterdam.

photoelectron flux can be assumed. The transmission efficiency measured in the laboratory was also found to be constant with energy over the range 3 to 88 eV. Instabilities in the beam produced by the electron monochromator when operated at very low currents and energies imposed the lower limit of reliable current measurements for these laboratory calibrations.

Although this electron monochromator can be used effectively to establish the energy scale, resolution, and transmission efficiency of the flight analyzer, it cannot be used for measurement of its geometric factor  $A\Omega$ . Measurement of this parameter requires an electron gun capable of providing a narrow beam of monoenergetic electrons that can be varied in angle and also translated so as to irradiate the entrance aperture of the analyzer incrementally throughout its angular acceptance range. A gun with these characteristics was being built but was not available for calibration of the present analyzer. The data presented in this report are, therefore, based on a calculated value of the geometric factor, and this calculation introduces the primary source of error in the measurements of photoelectron flux.

The electron gun mentioned above should provide an experimental determination of the geometric factor for future analyzers. This gun is similar to one developed by Lee<sup>17</sup> reportedly capable of providing a focused 15-eV beam of electrons within a spot diameter of less than 1 mm. At lower energies, the diameter of the beam increases somewhat approaching 1.5 mm at 4 eV. The beam currents reported are in the microampere range, which is well above that needed for calibration of the present analyzer. A reduction in beam current might possibly enhance the focusing characteristics of the gun.

## 5. VEHICLE INDUCED INTERFERENCE

The problem of data degradation caused by both solar illumination of the analyzer aperture area and by geomagnetic shadowing have already been mentioned. Under some conditions of orientation of the analyzer and geomagnetic field, where pitch angles are large, vehicle or payload components can intercept environmental electrons before they reach the analyzer aperture. In extreme cases, this orientation can cause photoelectrons produced from sunlit areas of the rocket or payload to enter the shaded analyzer aperture and contaminate the measurements. It is virtually impossible to correct the data degraded by these spurious photoelectrons. Armstrong<sup>18</sup> has described a computer program by which electron trajectories are

17. Lee, R.N. (1968) Electron gun for LEED applications, Rev. Sci. Instrum. 39:1306.

18. Armstrong, J.C. (1972) Spacecraft Interference with Low Energy Electron Measurements, Report CP 014, Applied Physics Lab., Johns Hopkins Univ., Silver Springs, Maryland.



calculated backward in time from the analyzer aperture over at least two Larmor periods to determine whether or not they would have intercepted the vehicle and whether such interceptions were in sunlit or shaded areas. The former case would indicate signal contamination by spurious photoelectrons, whereas the latter would identify signal degraded by vehicle interception. This program was applied to data obtained from the electron spectrometers aboard AE-C and AE-E to allow identification and elimination of anomalous data. These problems can be minimized by careful payload configuration and instrument orientation as described in Section 3. It is highly desirable that the axis of the entrance aperture be as nearly parallel as possible to the geomagnetic field lines. When this is accomplished, ambient electrons having paths within the acceptance angle of the aperture will have small pitch angles and will approach the entrance slit from directions nearly normal to the plane of its surface.

The vehicle potential, or skin charge  $V_S$ , which is generally negative, affects the measured energy spectra in two ways: First it introduces an energy loss to the incident electrons; secondly, it introduces a refractive effect on the trajectories of the incident electrons such that for negative  $V_S$  some electrons within the acceptance angle of the aperture that would be otherwise collected are lost. These two effects can produce misleading flux data, especially in the lower energy range. Although the correction for electron loss is not as straightforward as that for energy loss, a correction for the former can be made if an effectively large planar surface dominates the aperture area. The vehicle can be considered to be enveloped in a sheath in which an electric field gradient exists between the skin at the potential  $V_S$  and the undisturbed plasma. Equipotentials within this sheath follow the general contours of the vehicle components. In principle, refractive electron losses due to passage of electrons through the field established by the vehicle can be calculated by ray tracing and corrections applied to the data. When the instrument or vehicle structure in the vicinity of the aperture produces an irregular field in that area, ray tracing through the resulting complex equipotential surfaces can be of highly questionable accuracy. However, by locating the analyzer aperture on an effectively large planar surface with no structure protruding in the look direction, the equipotential contours become planar throughout the region subtended by the aperture. The electron paths through the field can then be traced easily as a function of energy and angle of incidence. An example of this calculated correction (see Appendix) for two apertures of different angular geometry is given in Figure 4. The figure shows curves based on electrons entering the sheath and within the given solid acceptance angles after passage through it. Further, the curves show the fraction of electrons collected as a function of their initial energy within solid acceptance angles of  $5^\circ$  and  $45^\circ$  after passage through fields associated with  $V_S$  values of  $-1.0$  and  $-2.0$  volts. Depending on the magnitude of  $V_S$ , these curves indicate that signal losses can commonly approach 20 percent in the 10 eV region of

ambient electron energy, exceed 50 percent in the 2-to 4-eV range, and rapidly approach complete loss at energies below this. The relatively small difference in the curves for the solid acceptance angles of  $5^\circ$  and  $45^\circ$  also indicates that opening the angular aperture to obtain greater signal intensity does not significantly increase the electron loss. These calculations will be verified experimentally when the electron gun and angular adjustment mechanism described earlier are available.

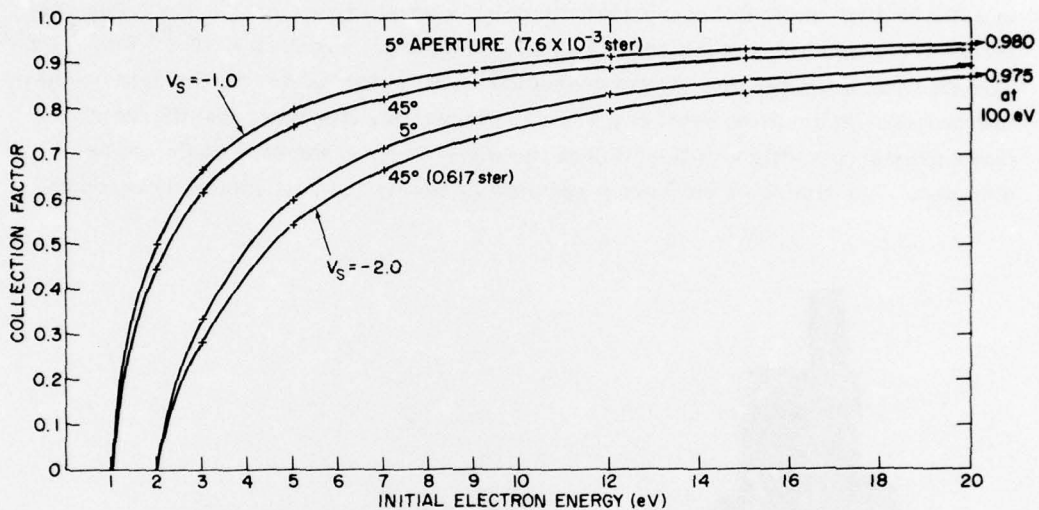


Figure 4. Illustration of Signal Loss Caused by the Refraction of Environmental Electrons during Passage through the Space Charge Sheath Surrounding a Planar Aperture. These curves show the collection factor, or fraction of electrons collected, as a function of initial (undisturbed) electron energy. The collection factor becomes unity in the absence of vehicle skin potential  $V_s$ . This factor is shown for two different solid angular apertures and two different values of  $V_s$ .

The measurement of photoelectron energy spectra and flux are obviously most difficult in the energy region below about 10 eV because both the vehicle charge and geomagnetic effects can introduce relatively much greater anomalies into the experimental data. However, as will be shown, the results of the present experiment indicate that a rocket-mounted  $127^\circ$  cylindrical electrostatic deflection energy analyzer, having a planar aperture surface that is carefully oriented with respect to its flight environment, has the potential of providing accurate data on the altitude dependence of low energy photoelectron fluxes. Further refinement of the low energy limit, the energy resolution, the stepping sequence, and the laboratory calibration of the analyzer should considerably enhance the accuracy of these measurements.

## 6. FLIGHT RESULTS

Figure 5 is a photograph of the rocket payload containing the electron analyzer mounted on the rear of the EUV spectrometer. The payload is shown in a simulated deployed position with the electron spectrometer axis directed downward and into the foreground. The entrance slit of the analyzer can be seen in the center of the aperture field plate A; the analyzer electronics is contained in the structure B just above. The flight was launched from White Sands Missile Range (WSMR), New Mexico at 1220:05 MST on 28 February 1976 reaching a peak altitude of 220 km. The solar zenith angle was  $42^\circ$  and the solar  $F_{10.7 \text{ cm}}$  emission was  $69.6 \times 10^{-22} \text{ Wm}^{-2} \text{ Hz}^{-1}$ . The electron analyzer operated successfully in all respects during the data acquisition period. Instrument recovery was not successful, however, and therefore a more precise post-flight calibration of the electron spectrometer could not be obtained. The timing of the launch resulted in nearly ideal alignment between the

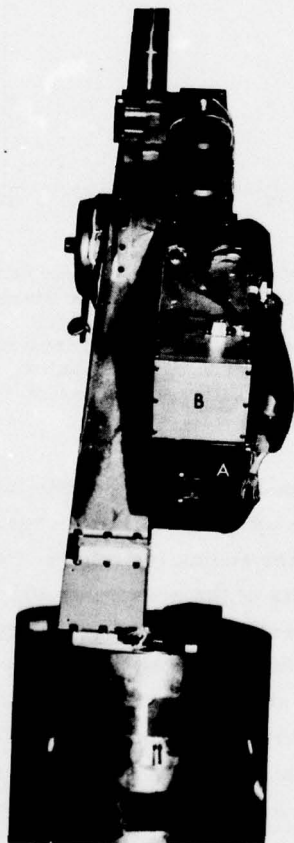


Figure 5. Photograph of the Payload Mounted in the Nose Section of an Aerobee 170 Prior to Flight. The experiment package is shown in simulated deployment with the electron analyzer axis directed downward and into the foreground. The entrance slit is located in the center of the aperture field plate A. The flight electronics is housed in the structure B just above



axis of the analyzer and the geomagnetic field. Because of the mounting configuration of the electron analyzer on the solar pointed spectrometer, the analyzer had a downward look angle of  $62^\circ$ . The geomagnetic dip angle at the WSMR surface is  $\sim 61^\circ$ . Therefore the angle between the axis of the analyzer and the magnetic field direction in the vertical plane was nearly zero. At the time of launch, the LHA at WSMR ( $106^\circ\text{W}$ ) was very close to  $0^\circ$ , and, because the local magnetic declination is  $\sim 12^\circ\text{E}$ , the resulting angular difference in the horizontal plane was approximately  $12^\circ$ .

During the data acquisition period of 235 sec, 184 complete energy scans were obtained. Examples of the raw data readout are given in Figure 6. The upper part of the figure shows the signal in counts per step recorded as a function of elapsed time in seconds after launch. The lower part of the figure shows the corresponding step numbers of the analyzer voltage  $V_A$  for the same intervals of elapsed time, where each step represents an energy increment  $\Delta E$  at energy  $E$ .

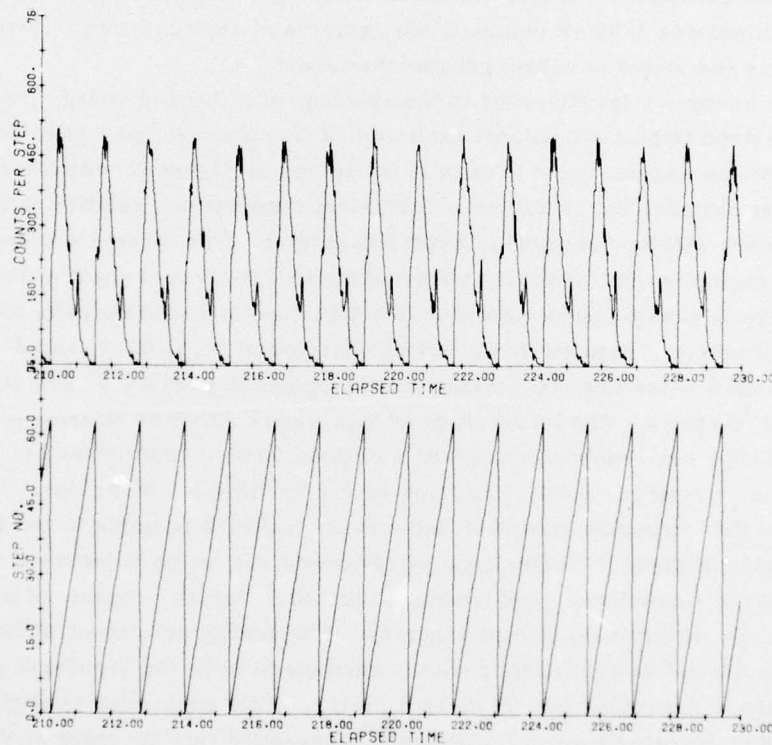


Figure 6. Example of Raw Data Readout Showing 15 Complete Energy Scans. The upper section gives raw counts per step (20 msec), while the lower section gives the corresponding step number (energy), both being plotted as a function of elapsed time, in seconds, after launch

The photoelectron flux measured at several altitudes is shown in Figure 7. The accuracy of actual flux values obtained by reduction of the measured data depends critically on the accuracy of analyzer calibration. Because of the limited accuracy of this calibration, the flux values in Figure 7 are only approximate. Relative values, however, can be considered accurately represented. No differences in the data were observed between up and downleg portions of the flight; in fact, spectra obtained at common altitudes during up and downleg segments were virtual replicas of each other. Three main features are evident in the energy spectra shown in this figure. These consist of a low energy valley appearing in the vicinity of 2.5 eV, a distinct peak in the region near 23 eV, and a relatively rapid decrease in flux values above 55 eV. All of these features are generally consistent with current theory and recent observations of Doering et al.<sup>6,7</sup> The curves have been corrected for an arbitrarily assumed vehicle potential of -1.0 V. No direct measurement of this potential was available in the flight, but, for reasons noted later, there is indication that the potential may have been slightly more negative than the assumed value of -1.0 V. Because the lower limit of energy sampled during this flight was 1.01 eV nominal, the energies of environmental electrons sampled were restricted to values greater than about 2 eV.

The low energy valley observed in the spectra, attributed to energy loss due to resonant electron impact vibrational excitation of  $N_2$ , appears most pronounced in the 130-to 150-km region, but it is seen in all curves of Figure 7, with the exception of the highest altitude, 217 to 219 km. Additional observations relative to this spectral feature will be discussed in more detail later. The structure shown in the 20-to 30-eV region is similar to that observed in the AE-C experiment of Doering et al.<sup>6</sup> There is general agreement that this structure is due principally to the production of primary photoelectrons having energies of 22.2, 23.9, and 27.2 eV, by the HeII-304 Å solar line that ionizes atomic oxygen to produce  $O^+$  ions in the  $^2P$ ,  $^2D$ , and  $^4S$  states. The latest observations aboard AE-E by Doering et al.<sup>7</sup> have shown this feature as resolved peaks with additional structure attributed to 25.2 eV photoelectrons produced in the formation of  $N_2^+$  by the same solar line. The resolution of this structure into identifiable peaks makes it possible to use the predicted energies of these photoelectrons as reference values for adjustment of the energy scales of such electron analyzers, a method potentially capable of providing in-flight energy calibrations of high accuracy. The energy resolution of the present analyzer has caused these distinct peaks to combine to form the broadened structure shown peaking at approximately 23 eV in Figure 7. This peak value is slightly lower than that expected from calculations<sup>4,6</sup> suggesting that the value of  $V_S$  was slightly more negative than the value of -1.0 eV used to correct the energy scale. The rapid decrease in the photoelectron flux at energies above about 55 eV is caused by the rapid decrease in solar flux in the short wavelength region of the spectrum.

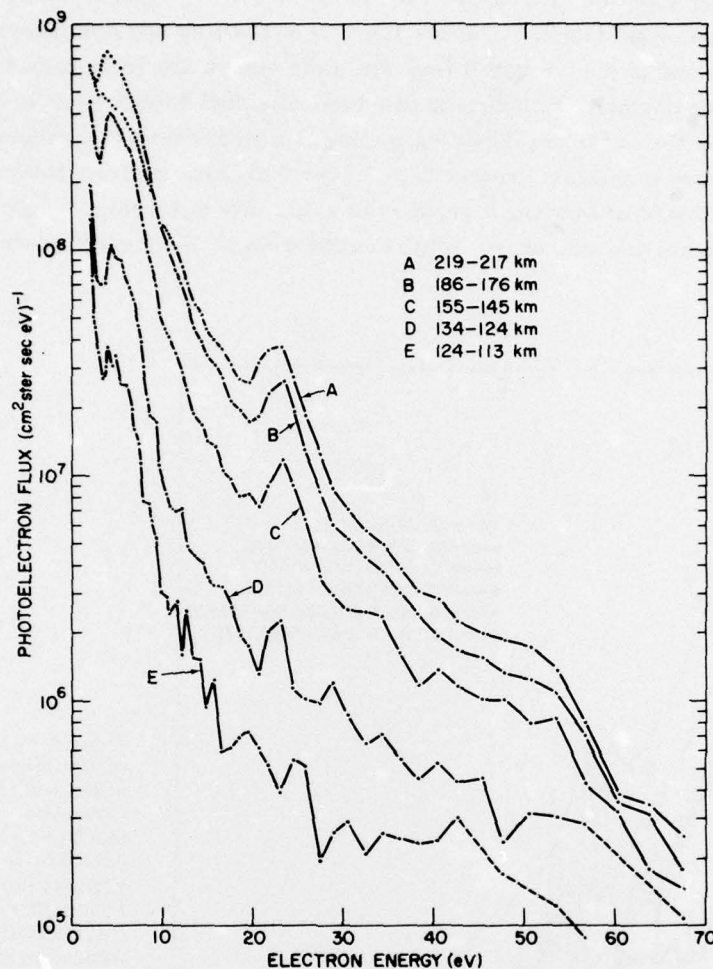


Figure 7. Photoelectron Flux as a Function of Electron Energy for Several Altitudes. These data have been corrected for an assumed vehicle potential of  $-1.0$  V. The assigned flux values are only approximate due to limitations in the preliminary calibration. This limitation does not apply to relative values of flux.

## 7. DISCUSSION

A comparison of these data with results obtained by other investigators is shown in Figure 8. With the exception of curve D which represents an average altitude of 230 km, these curves are from published data for the 180-to 200-km altitude range from five previous experiments in which four different instrumental measuring techniques were employed. Curve A was obtained with the present  $127^\circ$



deflection analyzer, curves B, C, and D with 180° spherical analyzers, curve E with a retarding potential analyzer,<sup>19</sup> and curve F with a "hyperbolic analyzer of the retarding potential type".<sup>8</sup> Curves B and D of Doering and coworkers are from data obtained in the AE satellites, while the others are from rocket experiments. A more complete comparison of these individual experiments is given in Table 1. While the curve representing the present study shows flux values generally higher by a factor somewhat greater than 2 over that obtained from the most recent satellite experiment of Doering's group (curve B), this difference cannot be considered significant because of the limited calibration of the present analyzer.

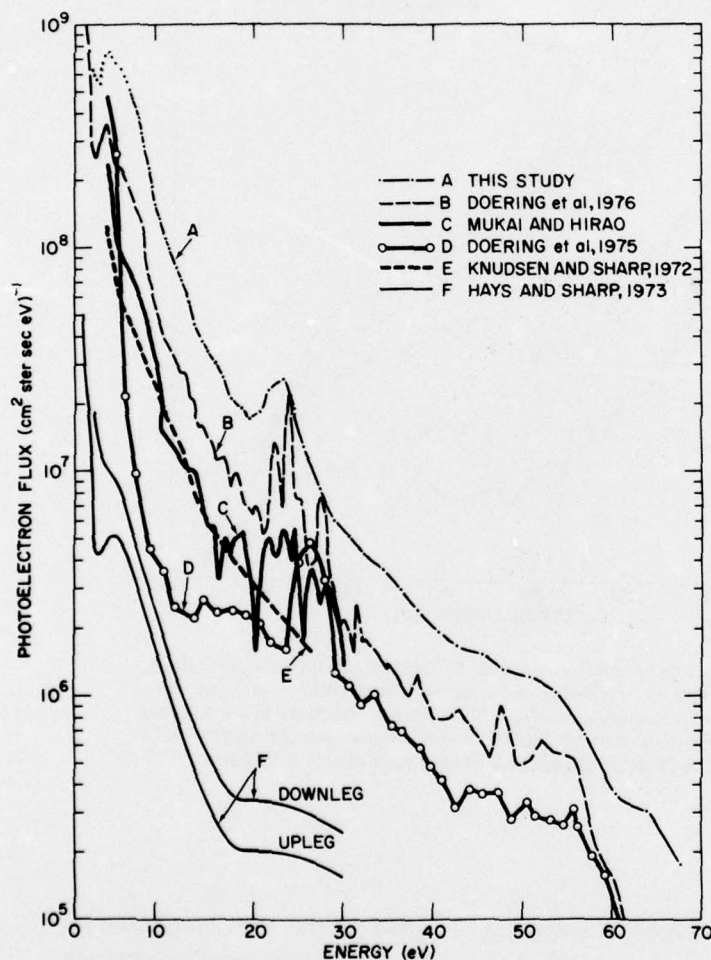


Figure 8. Comparison of the Present Results with Those Obtained by Others for the 180-to 200 km Altitude Region. A comparison of the relevant details of the individual experiments is given in Table 1

19. Knudsen, W. C., and Sharp, G. R. (1972) Eclipse and noneclipse differential photoelectron flux, *J. Geophys. Res.* 77:1221.

Table 1. Comparison of Experimental Details for Six Measurements of Electron Energy Spectra in the ~180-to 200-km Altitude

Study	Analyzer	Vehicle	Site-Time	Altitude (km)	SZA (deg)	10.7 cm Flux (Wm <sup>-2</sup> Hz <sup>-1</sup> )
(A) Present study	127° cylindrical electrostatic deflection	Rocket	WSMR 24 February 1976 1220 MST	182	42	$69.6 \times 10^{-22}$
(B) Doering et al (1976)	180° spherical electrostatic deflection	Satellite	Orbit 394 Day 355 1975 (20 December)	182	50	$69.7 \times 10^{-22}$
(C) Mukai and Hirao (1973)	180° spherical electrostatic deflection	Rocket	Uchinora, Japan 20 September 1972 1400 JST	200	43	$113 \times 10^{-22}$
(D) Doering et al (1975)	180° spherical electrostatic deflection	Satellite	Orbit 633 Day 42 1974 (11 February)	252-209	76 (Avg.)	$77.5 \times 10^{-22}$
(E) Knudsen and Sharp (1972)	Retarding potential (planar)	Rocket	Wallops I. 6 March 1970 1336 EST	180	47	$167.8 \times 10^{-22}$
(F) Hays and Sharp (1973)	HARP*	Rocket	WSMR 8 February 1971 Dawn	202	90	$123.2 \times 10^{-22}$

\* Acronym for hyperbolic analyzer of the retarding potential type. (See reference.)

The low energy valley in the 2 to 4-eV region of the spectra warrants some additional discussion. This feature has been observed in more detail in the present study than previously seen. It is of interest as a possible indicator of important thermospheric parameters such as the vibrational temperature and neutral density of  $N_2$ .<sup>2, 20</sup> The data obtained in the present experiment as a function of altitude are shown in expanded scale in Figure 9. These curves were obtained by integrating several consecutive energy scans over the altitude ranges indicated in the figure. The valley in the electron flux is apparent throughout the approximate altitude range 130 to 200 km and disappears above about 210 km. Its disappearance in this altitude region has been attributed to depletion of thermospheric  $N_2$ .<sup>7</sup>

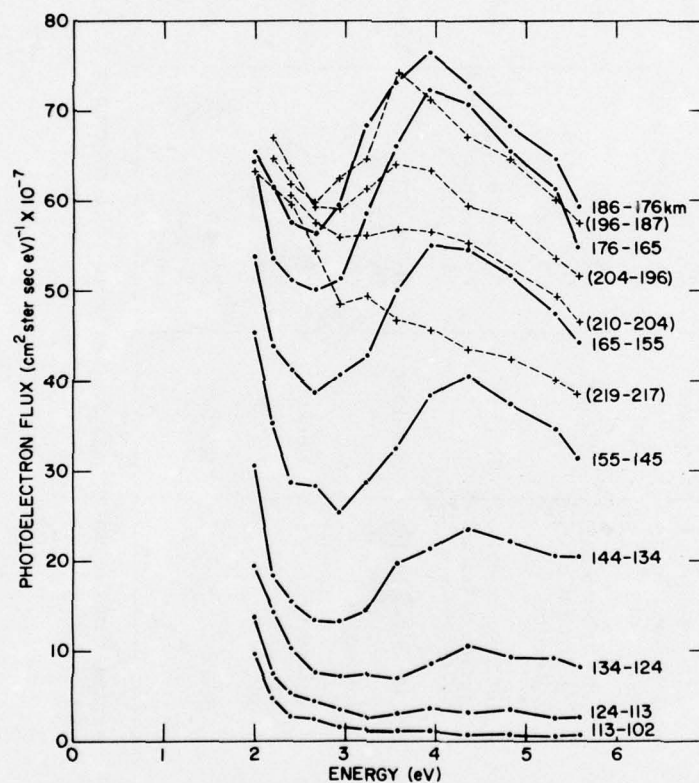


Figure 9. Energy Spectra between 2 and 5.6 eV as a Function of Altitude. The curves represent data obtained by integrating consecutive scans over the altitude ranges indicated. The valley-like structural feature attributed to  $N_2$  vibrational excitation losses appears as most prominent in the altitude range between approximately 140 and 190 km, and diminishes at both higher and lower altitudes

20. Jasperse, J. R., Private communication.



Ashihara and Takayanagi<sup>2</sup> relate this disappearance to a gradual smoothing process arising from a growing dominance of electron-electron collisions, while Jasperse<sup>4</sup> ascribes it principally to thermal electrons filling in the valley region as altitude increases. Figure 9 also shows this spectral feature diminishing with decreasing altitude. Doering et al<sup>7</sup> report similar results from their AE-E experiment, but their data were limited to altitudes above 154 km corresponding to the perigee of the satellite orbit. The solar zenith angles in their experiment varied somewhat for different altitudes because of orbit characteristics; this angle remains constant with altitude in the present rocket experiment.

The peak-to-valley ratios obtained from the data of Figure 9 are plotted in Figure 10 along with the ratios extracted from the AE-E data of Doering's group. The highest ratio obtained in the present experiment was approximately 1.7 at the altitude range 133 to 144 km. The ratios extracted from Doering et al near 160 to 170 km are, as shown, similar to the values obtained in the present experiment. However, the remaining values derived from these limited data indicate ratios diminishing more rapidly than ours for both higher and lower altitudes. Equivalent ratios extracted from the calculated data of Ashihara and Takayanagi<sup>2</sup> are higher than our measurements by more than an order of magnitude and, while their ratios diminish as altitude increases, they exhibit values greater than 1.0 up to 250 km. In comparison, the peak-to-valley ratios calculated by Jasperse<sup>4</sup> are substantially smaller, and the structure disappears entirely at 210 km, in good agreement with our observation. Jasperse's calculated ratios are larger than our observed values by a factor of about 3 at 130 km and by about 2 at 170 km. This apparent difference may result from the previously mentioned gaps between energy sampling steps which exist below 4.6 eV in the present experiment, or may also be in part the result of imprecisely known parameters which were necessarily used in the theoretical model. Despite these differences, there appears to be general agreement that the prominence of this feature varies inversely with altitude between some upper and lower limit. The lower limit, however, raises an additional question. Both theoretical studies cited which treat this feature in some detail indicate it to be most prominent at the lowest altitude calculated, 120 km (Ashihara and Takayanagi) and 130 km (Jasperse). Results from the present experiment, shown in Figure 10, indicate that the maximum ratio occurs at about 139 km, following which it is seen to drop rapidly as altitude decreases, disappearing again at about 108 km. More recently, Jasperse<sup>20</sup> has made some preliminary calculations for altitudes below 130 km, which suggest that such a reversal of ratio values could be explained by N<sub>2</sub> vibrational temperatures being substantially higher than kinetic temperatures. However, the assignment of values for vibrational temperatures as model parameters is necessarily a matter of theoretical estimate, and also of some

disagreement,<sup>21</sup> since actual measurements are not available. More refined in situ measurements may help to clarify this point, as well as to provide useful information relating to other parameters associated with thermospheric N<sub>2</sub>.

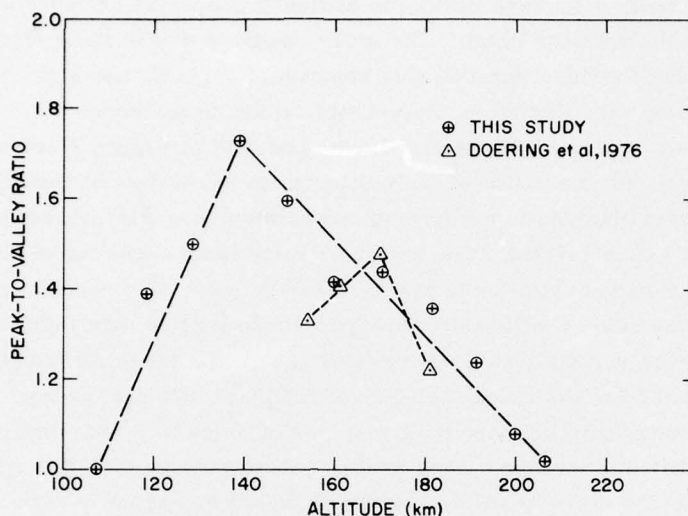


Figure 10. Ratios of Peak-to-valley Photoelectron Flux as a Function of Altitude. Peak and valley fluxes refer to values measured near 4 and 2.5 eV, respectively;  $\oplus$  = data from the present study;  $\Delta$  = data extracted from Doering et al (1976). The dashed lines are intended only as a coarse outline of the apparent trend in these data for each experiment. The solar zenith angle for the present study was constant at 42° and the solar F<sub>10.7</sub> cm emission was  $69.6 \times 10^{-22} \text{ Wm}^{-2} \text{ Hz}^{-1}$ . A linear extrapolation of the information provided by Doering et al (1976) indicates that their data were obtained for SZA values which varied from about 73° to 76° as altitude decreased over the range shown. The F<sub>10.7</sub> cm emission at the time of their measurements was  $72.8 \times 10^{-22} \text{ Wm}^{-2} \text{ Hz}^{-1}$ . It should be noted that these values are not the same as those referenced to the same authors in Table 1 for their spectrum in Figure 8; the latter measurements were made during a different orbital period

21. Breig, E.L., Brennan, M.E., and McNeal, R.J. (1973) Effect of atomic oxygen on the N<sub>2</sub> vibrational temperature in the lower thermosphere, *J. Geophys. Res.* 78:1225.

## References

1. Cicerone, R.J., Swartz, W.E., Stolarski, R.S., Nagy, A.F., and Nisbet, J.S. (1973) Thermalization and transport of photoelectrons: A comparison of theoretical approaches, J. Geophys. Res. 78:6709.
2. Ashihara, O., and Takayanagi, K. (1974) Velocity distribution of ionospheric low energy electrons, Planet. Space Sci. 22:1201.
3. Victor, G.A., Kirby-Docken, K., and Dalgarno, A. (1976) Calculations of the equilibrium photoelectron flux in the thermosphere, Planet Space Sci. 24:679.
4. Jasperse, J.R., Electron distribution function and ion concentration in the earth's lower ionosphere from Boltzmann-Pokker-Planck theory, (to be published).
5. Mukia, T., and Hirao, K. (1973) Rocket measurement of the differential energy spectrum of photoelectrons, J. Geophys. Res. 78:8395.
6. Doering, J.P., Peterson, W.K., Bostrom, C.O., and Armstrong, J.C. (1975) Measurement of low energy electrons in the day airglow and dayside auroral zone from Atmosphere Explorer C, J. Geophys. Res. 80:3934.
7. Doering, J.P., Peterson, W.K., Bostrom, C.O., and Potemra, T.A. (1976) High resolution daytime photoelectron energy spectra from AE-E, Geophys. Res. Lett. 3:129.
8. Hays, P.B., and Sharp, W.E. (1973) Twilight airglow photoelectrons and [OI] 5577-angstrom radiation, J. Geophys. Res. 78:1153.
9. Purcell, E.M. (1938) The focusing of charged particles by a spherical condenser, Phys. Res. 54:818.
10. Simpson, J.A. (1964) High resolution, low energy electron spectrometer, Rev. Sci. Instrum. 35:1698.
11. Kuyatt, C.E., and Simpson, J.A. (1967) Electron monochromator design, Rev. Sci. Instrum. 38:103.



## References

12. Hughes, A.L., and Rojansky, V. (1929) On the analysis of electron velocities by electrostatic means, Phys. Res. 34:284.
13. Roy, D., and Carette, J.D. (1971) Electrostatic spectrometers, Part III, Can. J. Phys. 49:2138.
14. McMahon, W., and Heroux, L. (1974) Measurement of energy and angular distribution and extreme ultraviolet photoelectrons, Appl. Opt. 13:438.
15. Feuerbacher, B., and Fitton, B. (1972) Experimental investigation of photoemission from satellite surface materials, J. Appl. Phys. 43:1563.
16. Kerwin, L., Marmet, P., and Carette, J.D. (1969) High resolution electron beams and their application, in Case Studies in Atomic Physics I, by E.W. McDaniel and M.R.C. McDowell, Ed., North-Holland Publishing Co., Amsterdam.
17. Lee, R.N. (1968) Electron gun for LEED applications, Rev. Sci. Instrum. 39:1306.
18. Armstrong, J.C. (1972) Spacecraft Interference with Low Energy Electron Measurements, Report CP 014, Applied Physics Lab., Johns Hopkins Univ., Silver Springs, Maryland.
19. Knudsen, W.C., and Sharp, G.R. (1972) Eclipse and noneclipse differential photoelectron flux, J. Geophys. Res. 77:1221.
20. Jasperse, J.R., Private communication.
21. Breig, E.L., Brennan, M.E., and McNeal, R.J. (1973) Effect of atomic oxygen on the N<sub>2</sub> vibrational temperature in the lower thermosphere, J. Geophys. Res. 78:1225.
22. Klemperer, O., and Barnett, M.E. (1971) Electron Optics, 3rd ed., Cambridge University Press, London, p. 5.

## Appendix A

### Correction for Refractive Signal Losses Due to Vehicle Skin Charge

It is a well-established principle of electron optics that an electron passing through an electrostatic field can be treated as having an index of refraction which, for practical purposes, can be expressed as  $N = (V)^{1/2}$  in electron volts.<sup>22</sup> Equipotentials within the field can be considered as refracting surfaces and the path of an electron can be traced through the field, divided into a number of equipotential steps, by repeated application of Snell's law. This method is as accurate as, and much simpler than, other techniques of ray tracing for simple axially symmetric fields. In the present application, it is not necessary to divide the field into a series of equipotential surfaces. Here we consider a charged sheath existing between the planar surface of the aperture field plate (AFP) at a potential  $V_s$  and the undisturbed environment. The source can then be considered as infinitely extended and, given isotropic distribution of thermospheric electrons, the actual depth of the sheath becomes unimportant so long as planar equipotentials can be assumed. In these circumstances, a single refracting surface is sufficient for purposes of calculation, since the angles at which refracted electrons approach the AFP surface is a function only of their angles of incidence at entry into the  $V_s$  sheath boundary and their energy with respect to the field potential. This relationship can then be expressed as:

$$\sin \alpha_i = \left( \frac{V_i - V_s}{V_s} \right)^{1/2} \sin \alpha_s$$

22. Klemperer, O., and Barnett, M.E. (1971) Electron Optics, 3rd ed., Cambridge University Press, London, p. 5.

where  $\alpha_i$  and  $\alpha_s$  are angles of sheath-boundary incidence and AFP-surface incidence, respectively, and  $V_i$  is the initial (undisturbed) potential of the electron prior to its passage through the negative space charge sheath -  $V_s$ . For a solid angle of acceptance having the dimensions  $(\alpha_s)(\beta_s)$ , the number of electrons collected  $n(e)_s$  as a function of the number that would have been collected  $n(e)_i$  in the absence of vehicle skin charge is

$$n(e)_s = \left( \frac{\alpha_s}{\alpha_i} \right) \left( \frac{\beta_s}{\beta_i} \right) n(e)_i .$$